Modeling Blowdown of Cylindrical Vessels Under Fire Attack

Haroun Mahgerefteh, Gboyega B. O. Falope, and Adeyemi O. Oke
Dept. of Chemical Engineering, University College London, London WC1E 7JE, U.K.

A robust numerical simulation is presented for predicting the risk of rupture during emergency depressurization or blowdown of cylindrical vessels containing high-pressure two-phase hydrocarbon mixtures under fire attack. Accounting for nonequilibrium effects between the constituent fluid phases, the model simulates the triaxial transient thermal and pressure stress profiles generated in both the wetted and unwetted wall sections of the vessel. A comparison of this information with the vessel material of construction temperature/yield stress data allows the precise evaluation of the risk of failure and, if applicable, the rupture mode during depressurization. Finally, based on the application of the model to a real system, the subtle differences between the failure risks associated with blowdown under fire as compared to those under ambient conditions are presented and discussed in detail.

Introduction

In the oil and gas industries, highly flammable pressurized hydrocarbon inventory is often stored and transported in cylindrical vessels. This poses the combined risks associated with high pressures, as well as storage of large quantities of flammable inventory. Blowdown, or the rapid intentional depressurization of such vessels, is often a common way of reducing the consequences associated with the above risks in an emergency situation.

However, the relatively rapid quasi-adiabatic expansion process during blowdown leads to significant fluid and, hence, vessel wall temperature drops (Haque et al. 1992a; Mahgerefteh and Wong, 1999). Should the wall temperature fall below the ductile-brittle transition temperature of the vessel wall material, rupture is likely to occur. This poses an imminently important question as to what the optimum depressurization rate should be in order to allow the fastest possible evacuation rate without running the risk of vessel rupture.

The modeling of blowdown is especially complex, requiring detailed consideration of several competing and often interacting heat-transfer, mass-transfer and thermodynamic processes. Despite this, in recent years, several models simulating the depressurization process with different degrees of sophistication have been proposed. The simplest and the most commonly used methods simulate the expansion of the fluid inside the vessel as either an isentropic or isenthalpic process (see, for example, API 521) (American Petroleum Institute, 1990b), thus leading to hopelessly unrealistic low vessel wall temperatures. This is, in turn, manifested in escalating capital equipment costs due to the requirement for specialized materials of construction.

By far the most comprehensive blowdown model to date accounting for most of the important processes taking place during blowdown was reported by Haque et al. (1992a) and later extended by Mahgerefteh and Wong (1999). However, although extensively validated against experimental data, the simulation is limited to blowdown under ambient surroundings only.

The above is an important drawback, as the most likely and catastrophic blowdown scenario would in fact involve a fire. The combination of the external impinging heat load and the resulting fluid expansion induced internal temperature drop introduces severe temperature stress gradients across the vessel wall. Apart from the above, any such modeling must also take account of the accompanying triaxial pressure stresses due to the pressurized inventory, as well as the thermal weakening of the vessel wall.

The capability to quantitatively evaluate the risks associated with blowdown under fire is particularly timely (Mahgerefteh et al., 1997, 1999, 2000) considering that envi-

Correspondence concerning this article should be addressed to H. Mahgerefteh.

ronmental groups in the U.S. are currently pressing for legislation to allow citizens to file lawsuits against high-pressure pipelines that pose "imminent and substantial endangerment to health or the environment" (Barlas, 1999). In the event of its success, it is only a matter of time before the same legislation is extended to hydrocarbon storage vessels particularly since these are frequently used for storage of domestic fuel gases in populated areas.

There is indeed ample experimental evidence demonstrating the very real risk of vessel rupture during blowdown un-

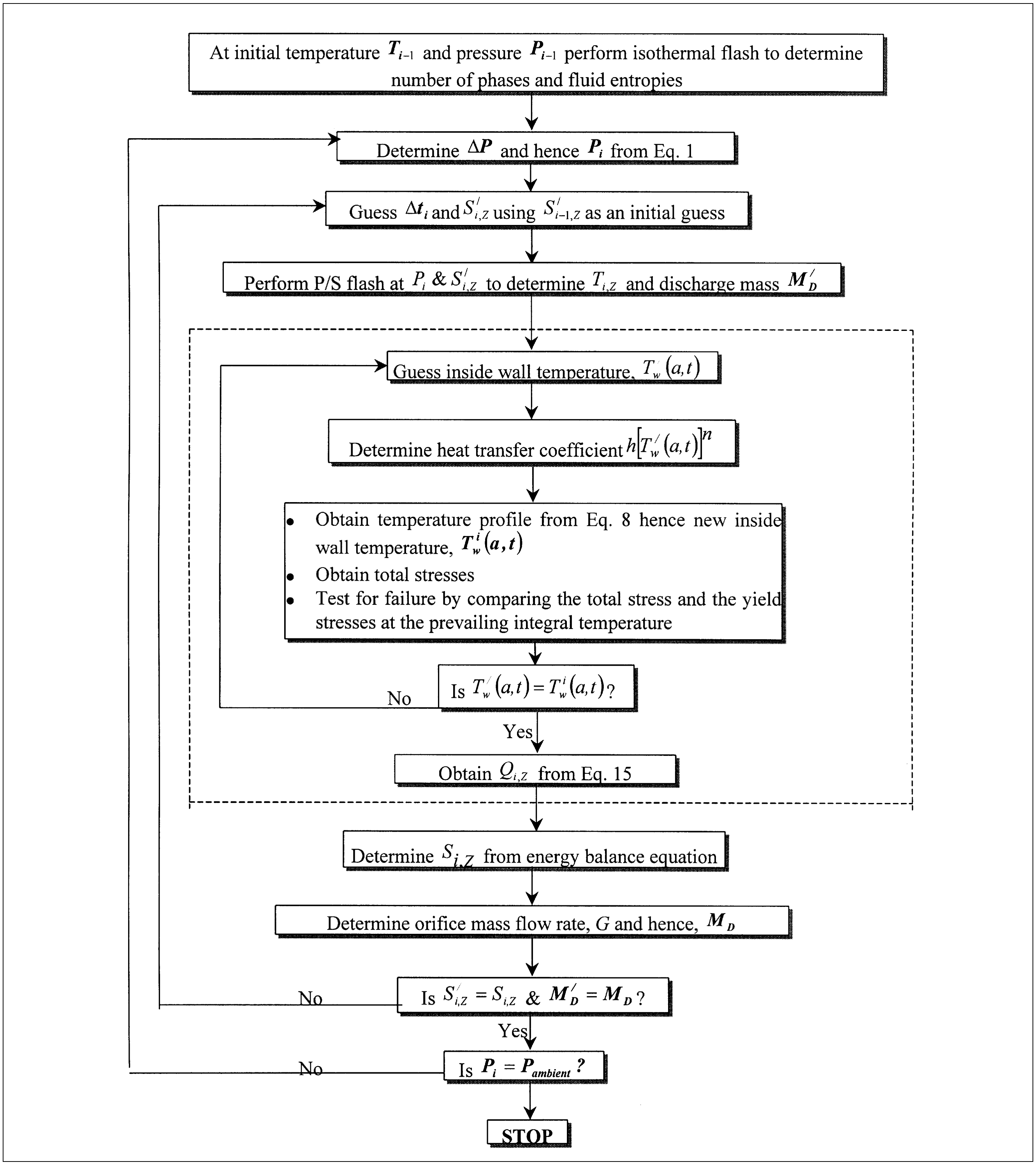

Figure 1. Calculation flow logic diagram for blowdown under fire.

der fire (Birk, 1995, 1988; Sumathipala et al., 1992; Kielec and Birk, 1997).

It is worth noting that in recent years some work relating to the simulation of pressure relief valve depressurization under fire and ambient conditions has been reported. For example, general empirically based guidelines on valve relief sizing under fire are provided by the American Petroleum Institute (1990a) (API Recommended Practice, 520). However, apart from gross simplifying assumptions, the procedure is open to interpretation by the user. The Split Fluid blowdown model by Overa et al. (1994) on the other hand, while considering the effect of fire, critically ignores wall temperature gradients.

Beynon et al.'s (1988) HEATUP model simulates the depressurization of horizontal LPG vessels engulfed by fire. Complete fire engulfment is treated with a vertically varying, time-dependent heat flux. However, although the wall temperature gradients are accounted for, the associated thermal and pressure stress gradients are ignored.

The ENGULF computer programs ENGULF I and II (Hunt and Ramskill, 1985; Ramskill, 1988) also exist for temperature and pressure predictions within a tank partly filled with liquid. The former simulates a complete fire engulfment scenario, while the latter accounts for partial engulfment. Both consider wall temperature distribution effects, but assume single-phase discharge with ideal gas behavior for the vapor phase. Additionally, similar to the HEATUP, ENGULF models do not evaluate the risk of rupture under impinging heat loads by predicting the associated vessel wall thermally induced stresses.

In this article, we present the development of a rigorous numerical simulation for the quantitative risk assessment of rupture following the blowdown of cylindrical vessels containing high-pressure hydrocarbon mixtures engulfed by fire. The results of the simulation, based on the application of the model to a hypothetical case, are used to quantitatively elucidate the subtle differences between the risks associated with blowdown under fire as opposed to those under ambient conditions. Apart from the triaxial transient stresses within the three-dimensional (3-D) cylindrical axes, typical simulated data include temperature/time variations for the wetted and unwetted walls, as well as those for bulk liquid and vapor. The risk of rupture is determined by comparison of the total pressure and thermal stresses with the vessel's material of construction yield stress data.

Model Development

Blowdown simulation

The simulation of the various important processes taking place within the pressurized inventory during blowdown under fire is performed by incorporating the pertinent transient thermal and pressure stress effects into our ambient BLOWSIM model (Mahgerefteh and Wong, 1999). Figure 1 shows the corresponding calculation flow logic diagram.

Briefly, the model accounts for nonequilibrium effects between phases, heat transfer between each fluid phase and their corresponding sections of vessel wall, interphase fluxes due to evaporation and condensation, and the effects of sonic flow at the orifice. It has been extensively validated (Mahgerefteh and Wong, 1999) against published experimental data (Szczepanski, 1994) obtained in conjunction with the ambient blowdown of a vessel containing pressurized multicomponent hydrocarbon inventory.

Reducing pressure steps are used to numerically simulate the depressurization process with the pressure increment ΔP_i at a subsequent pressure interval given by

$$\Delta P_i = P_{i-1} \times r \tag{1}$$

with the pressure ratio r being equal to 0.05. The advantages of employing pressure increments are its thermodynamic convenience and computational efficiency as opposed to choosing time intervals (Hunt and Ramskill, 1985; Ramskill, 1988; Overa et al., 1994), which are thermodynamically irrelevant.

Thermodynamic and phase equilibrium data are generated using Peng-Robinson (Peng and Robinson, 1976) CEOS, as it has been shown to be particularly applicable to high-pressure hydrocarbon mixtures (deReuck et al., 1996; Assael et al., 1996). The number of phases present at any given time is determined using the Gibbs tangent plane stability test (Michelsen, 1982). Based on experimental observations by Moodie et al. (1988), it is assumed that both vapor and liquid are well mixed, negating the effects of temperature gradients within each constituent phase. Furthermore, pressure is assumed to be spatially uniform within the vessel.

The nonisentropic expansion of each fluid phase during blowdown is accounted for by assuming a polytropic expansion process (Bett et al., 1975) in which both heat and work are considered.

Returning to Figure 1, an iteration procedure is employed to obtain the time duration Δt and, hence, the entropy S_i at the end of each pressure step, such that the amount of material discharged as a result of the pressure drop from P_{i-1} to P_i corresponds to the inventory mass loss as a result of the entropy change from S_{i-1} to S_i. Pressure/entropy flash calculations at pressure P_i and entropy S_i are performed subject to the satisfaction of the pertinent material and energy balances. Z refers to the separated vapor or liquid phase within the vessel.

The fluid approaching a relief valve during depressurization can either be single- or two-phase. If the backpressure is sufficiently low, the fluid accelerates through the orifice at its maximum velocity and expands rapidly from the upstream to the orifice pressure. Consequently, condensation may occur, which results in two-phase flow. The procedure for determination of the discharge rate and the state of fluid phase at the orifice is described elsewhere (Haque et al., 1992a; Mahgerefteh and Wong, 1999). In essence, it is based on carrying out an energy balance across the orifice assuming isentropic expansion coupled with thermodynamic and phase equilibrium.

Vessel wall analysis

The transient radial wall temperature profile is obtained analytically by use of the method of separation of variables (Ozisik, 1980), as opposed to numerical solution methods (Beynon et al., 1988; Haque et al., 1992a). This is because the former allows the use of highly efficient adaptive integrators especially suited to oscillating, nonsingular integrands (NAG

Fortran Library). These render the analytical evaluation of the temperature profile with relative ease. Furthermore, the accuracy of the analytical method is not dependent on the number of temperature nodes employed, and, hence, the need for improved numerical accuracy by the use of finer wall grid nodes is eliminated.

The transient radial wall temperature profile $T(r,t)$ is obtained from the solution of the differential equation for radial heat conduction in a cylindrical co-ordinate system, subject to boundary conditions of the third and second kind for the internal and external surfaces, respectively.

In essence, $T(r,t)$ can be split into a homogeneous $T_h(r,t)$ and a steady-state component $T_s(r)$ such that

$$T(r,t) = T_s(r) + T_h(r,t) \tag{2}$$

The steady-state solution can be shown to be given by

$$T_s(r) = C_1 + C_2 \ln r \tag{3}$$

C_1 and C_2 are obtained by integration of the steady-state temperature profile such that

$$C_2 = \frac{bQ_f}{k} \qquad \& \, C_1 = T_Z - \frac{bQ_f \ln a}{k} + \frac{bQ_f}{ah_Z} \tag{4}$$

where a and b are the inside and outside cylinder radii respectively, Q_f is the external heat flux, k is the wall thermal conductivity, and h_{Zx}, the heat-transfer coefficient.

For the homogeneous component, the solution for the time variable function is given by

$$\Gamma(t) = \exp\left(-\alpha\beta_m^2 t\right) \tag{5}$$

where α is the thermal diffusivity.

The corresponding solution for the space variable function, based on solving the resulting eigenvalue problem is given by

$$\Gamma(s) = R_o(\beta_m, r) \tag{6}$$

where $R_o(\beta_m)$, $N(\beta_m)$ and β_m, respectively, refer to the eigenfunction, the norm, and the eigenvalues of the resulting eigenvalue problem. The expressions for these are given in the Appendix.

The complete homogeneous solution for $T_h(r,t)$ based on the linear superposition of the separated elementary solution and the application of the initial condition is given by

$$T_h(r,t) = \sum_{m-1}^{\infty} \frac{1}{N(\beta_m)} \exp\left(-\alpha\beta_m^2 t\right) R_o(\beta_m, r) \times \int_a^b r' R_o(\beta_m, r') F(r') dr' \tag{7}$$

where $F(r')$ is the temperature profile at $t = 0$.

The complete solution for the temperature profile is then obtained from Eq. 2 such that

$$T(r,t) = T_s(r) + \sum_{m=1}^{\infty} \left[\frac{1}{N(\beta_m)} \exp\left(-\alpha\beta_m^2 t\right) R_o(\beta_m, r) \times \int_a^b r' R_o(\beta_m, r') \left[T_o - T_s(r')\right] dr' \right] \tag{8}$$

The equations for evaluating the pertinent tangential, radial, and longitudinal thermal and pressure stresses for a closed-end pressurized vessel are given in the Appendix. For brittle thick-walled cylinders experiencing nonuniform heating such as that used in this study, rupture occurs when any one of the above triaxial total normal pressure and thermal stresses exceed the vessel material's yield stress (Popov, 1999).

Wall/fluid heat transfer

Based on experimental observations (Haque et al., 1992b; Overa et al., 1994; Moodie et al., 1988), both forced and natural convection govern the heat-transfer mode in the vapor phase during blowdown. The correlation by Petukhov and Popov (Perry and Green, 1997) with the fanning factor determined by an equation recommended by Filonenko (Perry and Green, 1997) is used to account for the forced convection. The free convection vapor-phase heat-transfer coefficient for the cylindrical section of the vessel in contact with the vapor on the other hand is obtained from the correlation by Churchill and Chu (Incropera and DeWitt, 1996). This correlation is applicable to the entire range of Rayleigh number (Incropera and DeWitt, 1996) thereby covering both laminar and turbulent flows. The McAdam's correlation (Incropera and DeWitt, 1996) is used to obtain the heat-transfer coefficient for either of the curved ends exposed to vapor. The Churchill and Chu (Incropera and DeWitt, 1996) and the McAdam's correlations (Incropera and DeWitt, 1996) approximate the curvature of the cylinder by assuming it as a plane of the same surface area as the cylinder. The radiative heat transfer due to the relatively high wall temperatures experienced in the dry walls (Moodie et al., 1988) is accounted for by using standard correlations (Incropera and DeWitt, 1996).

Heat transfer between the vessel wall and the liquid phase is governed by boiling heat transfer, the nature of which is determined by the excess temperature. Under fire conditions, nucleate, transition, and stable film boiling heat transfer may exist. However, experiments by Moodie et al. (1985) show that the critical heat flux beyond which transition boiling begins is not reached, therefore indicating the prevalence of nucleate boiling. For the sake of robustness, we account for whatever mode of boiling may result as determined by the excess temperature. The appropriate correlating equation for each boiling regime given by Incropera and De Witt (1996) is then used.

The amount of heat to either fluid phase is determined by an iterative procedure performed by employing the Numerical Algorithm Group (NAG) mathematical library routines (NAG Fortran Library) to solve the heat resulting heat-transfer equation. The routine locates the zero of the continuous function using a continuation method based on a secant iteration and uses reverse communication for the function evaluation. As indicated in Figure 1, this involves an initial guess of the unknown wall temperature $T_w^{\prime}(a,t)$ at time t, from which the heat-transfer coefficient $h[T_w^{\prime}(a,t)]^n$ is obtained from the correlations as given by Incropera and De Witt (1996). The radial temperature profile can then be obtained from Eq. 8 to give a new value for the inside wall temperature $T_w^i(a,t)$ subject to the following convergence

$$T_w^{\prime}(a,t) - T_w^i(a,t) \leq 10^{-3} \tag{9}$$

The fluid/wall heat transfer to either of the phases is then obtained from

$$Q = h\left[T_w^{\prime}(a,t)\right]^n \left[T_w^i(a,t) - T_Z\right] A \Delta t \tag{10}$$

where n is a power index depending on the heat-transfer coefficient used. A is the heat-transfer area, the subscript w refers to the wall, and T_Z is either the liquid or vapor temperature, as determined by the pressure/entropy flash calculation.

Results and Discussion

Inventory and pressure profiles

The following represents the results of the application of the above model to the blowdown of a carbon steel vessel containing a multicomponent hydrocarbon mixture containing 64 mol% C_1, 6 mol% C_2, 28 mol% n-C_3 and 2 mol% n-C_4. We choose this particular example as it relates to a real vessel for which actual blowdown data under ambient conditions are available (Szczepanski, 1994). These results were previously used to extensively validate our blowdown model under ambient conditions (Mahgerefteh and Wong, 1999). Since the exact type of steel used in Szczepanski's (1994) study was not given, for the sake of analysis, we assume it to be made carbon steel (BS 3100 AM1).

The vessel is at initial temperature and pressure of 293 K and 116 bara, respectively. Under these conditions, the hydrocarbon inventory is in the gaseous state although depressurization results in the formation of a two-phase mixture. The formation of liquid increases the rate of fluid/wall heat transfer, thus dramatically influencing the vessel's thermal response under fire attack.

The wall thickness is 59 mm with its length and inside diameter being 3.240 m (2.75 m tan-to-tan) and 1.130 m, respectively. An equivalent orifice diameter of 10 mm is used. Two types of blowdown scenarios are simulated, one with the vessel completely engulfed in a pool fire radiating a heat flux 90 kW/m^2 and the other under ambient conditions. The subtle differences between the results, as well as the quantitative risk assessment of vessel rupture, are described in detail as follows.

Temperature profiles

Figure 2 shows the predicted pressure and inventory/time profiles during blowdown under fire loading (curves A and D, respectively) and ambient surroundings (curves B and C, respectively). As it may be observed, fire results in a marked reduction in the rate of drop in pressure. For example, even after 1,200 s following blowdown, the residing pressure in the vessel is 10 bara. This is due to the significant amount of liquid boiling and evaporation, which are, in turn, manifested in a corresponding increase in the rate of loss in inventory.

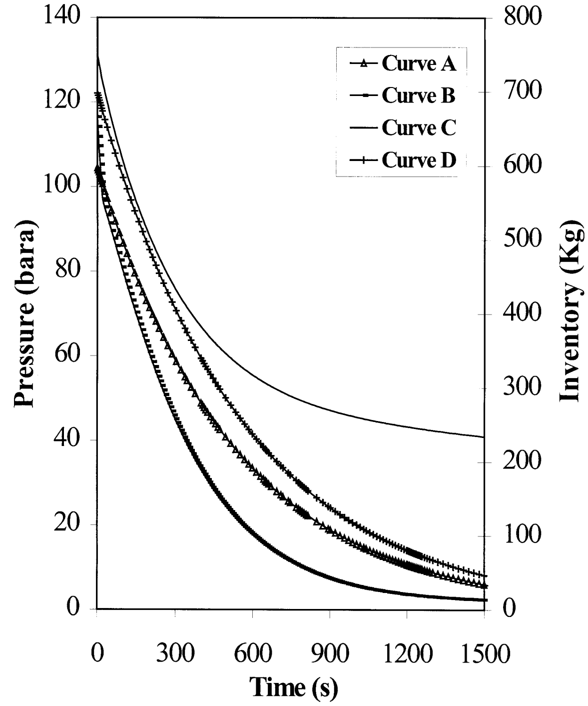

Figure 2. Pressure and inventory variations with time during blowdown under fire and ambient conditions.

Curve A: pressure, fire; Curve B: pressure, ambient; Curve C: inventory, ambient; Curve D: inventory, fire.

Figure 3 shows the variations in the unwetted inside vessel wall temperature (wall temperature in contact with the vapor, curve A) and vapor temperature (curve B) as a function of time during blowdown under fire attack. The corresponding data during blowdown under ambient conditions are also given (curves C and D). Figure 4 on the other hand shows the analogous results as in Figure 3, but for the liquid phase and wetted inside wall temperatures. The data for the liquid phase starts at approximately 38 s after the start of blowdown since this marks the onset of liquid condensation from the vapor phase.

In Figure 4, it is observed that in all cases, the fluid and the corresponding vessel wall follow similar time/temperature profiles. Referring to the results under ambient conditions in Figures 3 (curve D) and 4 (curve D), it is clear that blowdown results in a significant and similar order of magnitude (about 40 K) drop in both the vapor and liquid temperatures. However, due to the relatively poor mode of heat transfer, the wall temperature in contact with the vapor (Figure 3, curve C) remains relatively unchanged, whereas that in contact with the liquid (Figure 4, curve C) experiences a dramatic drop in temperature, bringing the vessel perilously close to brittle fracture. After 1,200 s following blowdown, the wetted wall temperature is in fact only 6 K above the ductile-brittle transition temperature of the vessel wall (about 244 K, Haque et al., 1992b).

The effect of fire is to counteract these temperature drops particularly in the vapor phase where a significant and mono-

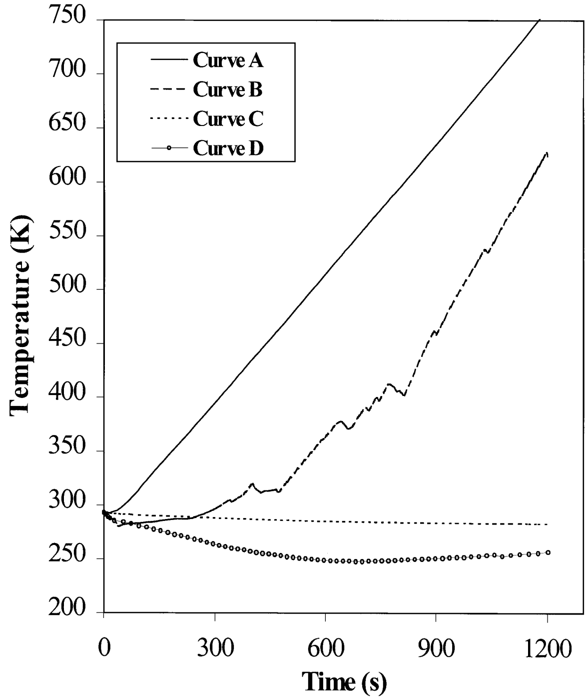

Figure 3. Unwetted inside wall and bulk vapor temperature profiles during blowdown under fire (90 kW/m^2) and ambient conditions.

Curve A: inside wall, fire; Curve B: bulk vapor, fire; Curve C: inside wall, ambient; Curve D: bulk vapor, ambient.

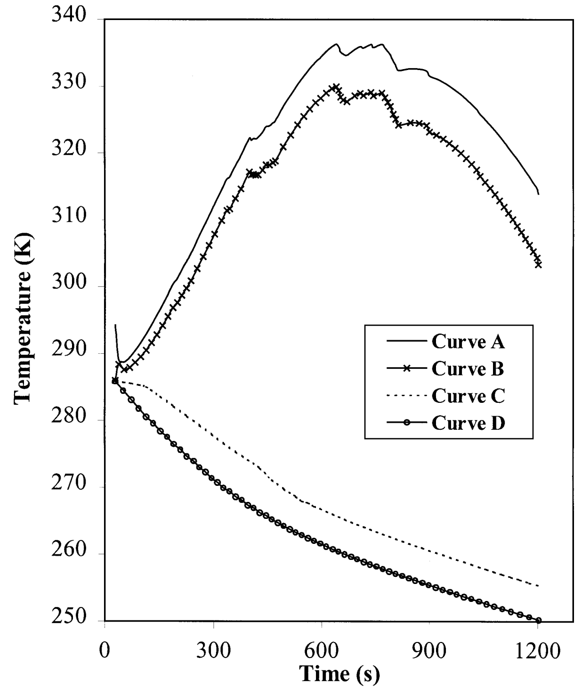

Figure 4. Wetted inside wall and bulk liquid temperature profiles during blowdown under fire (90 kW/m^2) and ambient conditions.

Curve A: inside wall, fire; Curve B: bulk liquid, fire; Curve C: inside wall, ambient; Curve D: bulk liquid, ambient.

tonic increase in temperatures of both the vapor (Figure 3, curve B) and the dry wall (Figure 3, curve A) are observed. According to these results, failure due to a ductile/brittle transition in the unwetted section of the vessel during blowdown under fire is impossible.

Returning to the wetted wall and liquid phase data under fire conditions (Figure 4, curves A and B), the initial increase in liquid temperature is due to the dominance of heat-transfer effects from the fire as opposed to cooling due to the liquid evaporation. At around 600 s following blowdown, the two modes of heat transfer switch roles and a continuous reduction in both the liquid and the corresponding wall temperature is observed. However, the final wall temperature still remains well above the ductile/brittle transition temperature of the vessel material (cf. 300 with 244 K). As such, the risk associated with brittle failure of the wetted wall during blowdown under fire is minimal.

It is noteworthy that under fire, the vapor inside wall temperature (Figure 3, curve A) reaches a significantly higher value than that in contact with the liquid (Figure 4, curve A, cf. 750 K as opposed to 340 K). This is due to the far lower heat-transfer coefficient in the vapor phase (5–200 W/m$^2 \cdot$K), compared to that in the liquid phase (1,000–20,000 W/m$^2 \cdot$K).

Figure 5 shows the variation of the temperature difference between the inner and outer walls for the wetted (curve A) and unwetted sections (curve B) of the vessel during blowdown under fire. As it is clear, the vessel wall in contact with the liquid inventory experiences a much larger temperature gradient compared to that exposed to the vapor. This is once again primarily a consequence of the much larger heat-transfer coefficient in the liquid phase, which in turn results in the rapid removal of heat from the inner vessel wall to the bulk liquid. The fact that the temperature gradient increases in magnitude with time is indicative of improved rate of heat transfer in the liquid phase as blowdown proceeds.

The greater temperature gradient in the wetted as compared to the unwetted wall on its own merit increases the risk of vessel rupture in the liquid space due to the resulting thermal stresses. On the other hand, although experiencing a much lower temperature gradient, the dry wall mean temperature at any given time during blowdown is far greater than that for the wetted wall. This effect in turn increases the risk of vessel failure due to the mechanical weakening of the vessel wall. To determine which of these two competing factors eventually results in the failure of the vessel requires a precise evaluation of the accompanying pressure and thermal stress profiles followed by comparison with the vessel material's yield strength at the prevailing conditions.

Thermal and pressure stress profiles: The evaluation of risk and mode of failure

Figures 6–8 show the simulated time-dependent variations of the total radial (Figure 6), tangential (Figure 7), and longitudinal stress profiles (Figure 8) for the unwetted and wetted vessel walls during blowdown under fire. The various stress profiles have been normalized with respect to the vessel material of construction's yield stress data (Brandes, 1983) at the

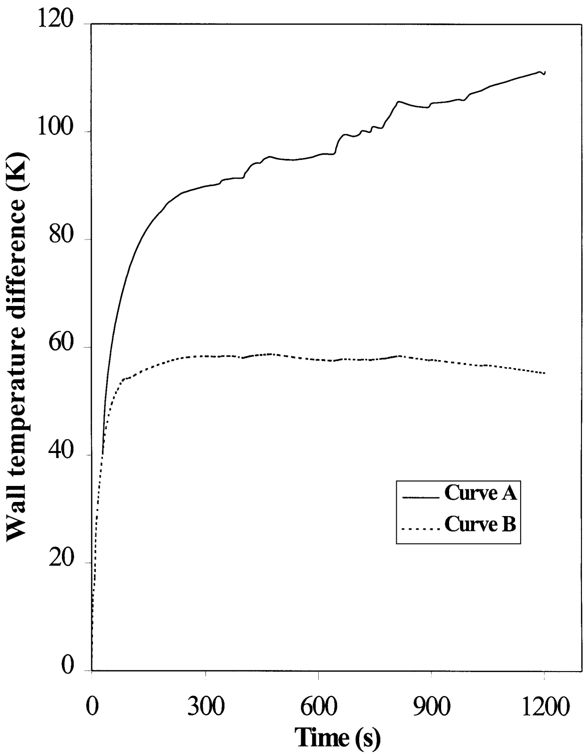

Figure 5. Variation of wetted and unwetted wall temperature difference with time during blowdown under fire.

Curve A: wetted wall; Curve B: unwetted wall.

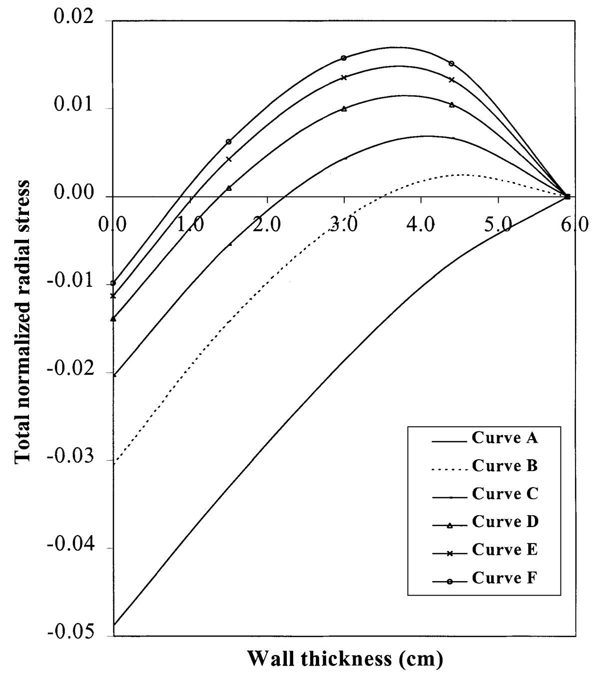

Figure 6a. Unwetted wall, normalized total radial stress profiles at different times during blowdown under fire.

Curve A: 10 s, $\Psi = 299.5$ K; Curve B: 300 s, $\Psi = 426.7$ K; Curve C: 600 s, $\Psi = 548.9$ K; Curve D: 900 s, $\Psi = 665.0$ K; Curve E: 1,100 s, $\Psi = 746.6$ K; Curve F: 1,200 s, $\Psi = 783.5$ K.

prevailing vessel integral temperature $\Psi(K)$. This is given by

$$\Psi(K) = \frac{\int_a^b T(r,t)}{b-a} \tag{11}$$

where a and b are the internal and external radii of the cylindrical vessel, respectively.

Normalized total stress values greater than unity indicate imminent vessel failure. Positive and negative values on the other hand represent tensile and compressive stresses, respectively.

Referring to Figures 6a and 6b, it is clear that vessel failure in the radial direction is extremely unlikely since normalized stress values remain well below unity. These stresses decrease with time, gradually transversing from purely compressive (due to pressure effects) to tensile (due to thermal effects) stresses as depressurization proceeds. Interestingly, the total radial stress is similar in both the wetted and unwetted sections of the vessel.

The data in Figures 7 and 8 on the other hand indicate much higher stresses in the tangential and longitudinal axes. In most cases, these are relatively uniform across the wall thickness at the onset of depressurization. However, as depressurization proceeds, the stress gradients become much steeper exposing the vessel walls to both compressive (at the outer walls) and tensile (at the inner walls) forces. At any

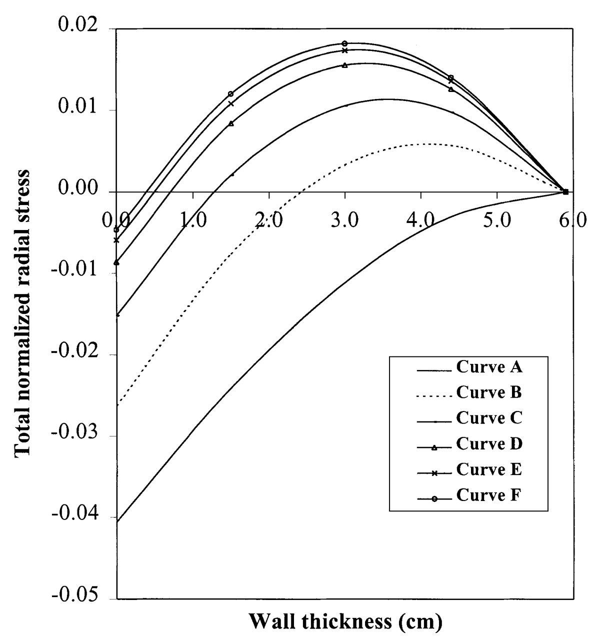

Figure 6b. Wetted wall normalized total radial stress profiles at different times during blowdown under fire.

Curve A: 38 s, $\Psi = 309.1$ K; Curve B: 300 s, $\Psi = 358.4$ K; Curve C: 600 s, $\Psi = 383.9$ K; Curve D: 900 s, $\Psi = 385.0$ K; Curve E: 1,100 s, $\Psi = 377.3$ K; Curve F: 1,200 s, $\Psi = 371.5$ K.

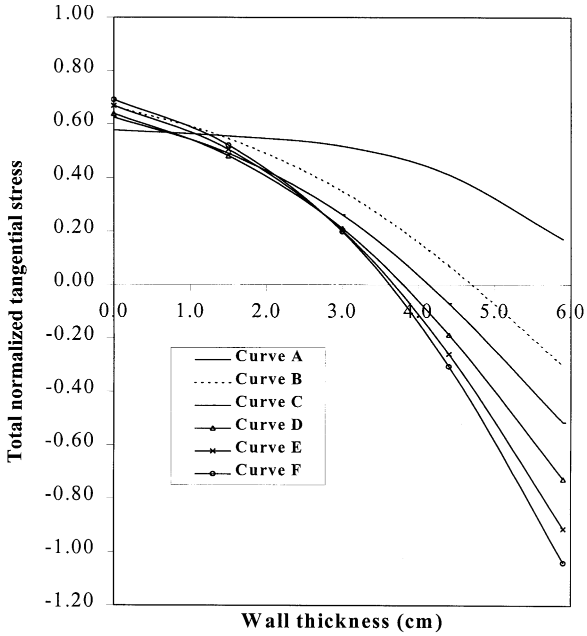

Figure 7a. Unwetted wall normalized total tangential stress profiles at different times during blowdown under fire.

Curve A: 10 s, Ψ = 299.5 K; Curve B: 300 s, Ψ = 426.7 K; Curve C: 600 s, Ψ = 548.9 K; Curve D: 900 s, Ψ = 665.0 K; Curve E: 1,100 s, Ψ = 746.6 K; Curve F: 1,200 s, Ψ = 783.5 K.

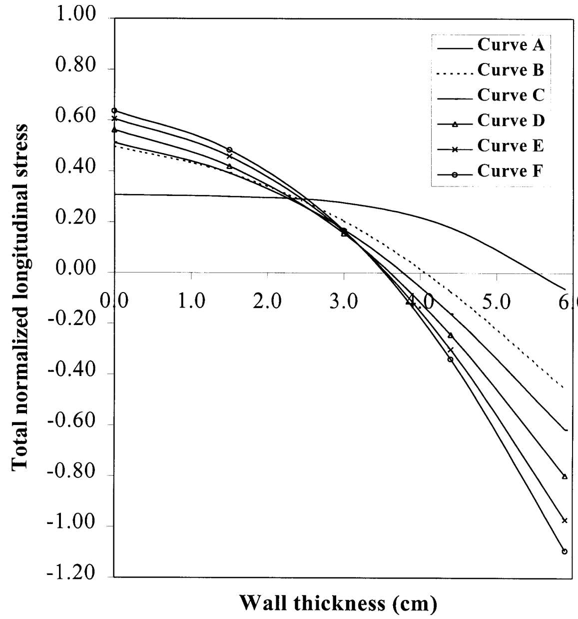

Figure 8a. Unwetted wall normalized total longitudinal stress profiles at different times during blowdown under fire.

Curve A: 10 s, Ψ = 299.5 K; Curve B: 300 s, Ψ = 426.7 K; Curve C: 600 s, Ψ = 548.9 K; Curve D: 900 s, Ψ = 665.0 K; Curve E: 1,100 s, Ψ = 746.6 K; Curve F: 1,200 s, Ψ = 783.5 K.

given time, these forces are greater in the longitudinal direction, eventually resulting in rupture propagating from the outer wall of the unwetted section of the vessel some 1,100 s following blowdown under fire. This is in contrast to the

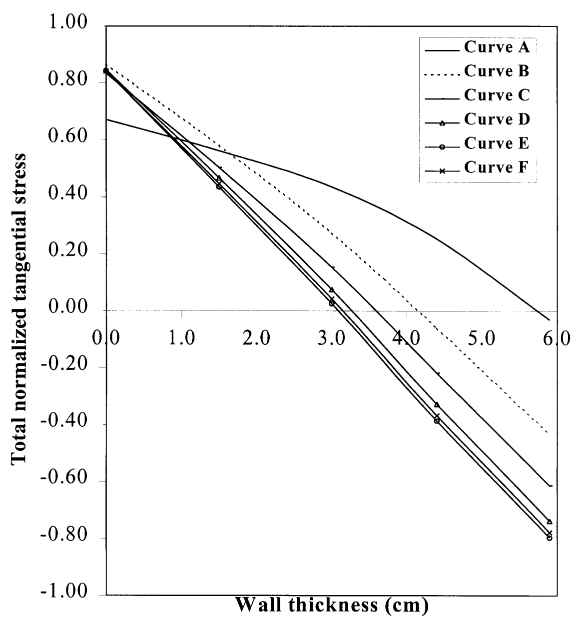

Figure 7b. Wetted wall normalized total tangential stress profiles at different times during blowdown under fire.

Curve A: 38 s, Ψ = 309.1 K; Curve B: 300 s, Ψ = 358.4 K; Curve C: 600 s, Ψ = 383.9 K; Curve D: 900 s, Ψ = 385.0 K; Curve E: 1,100 s, Ψ = 377.3 K; Curve F: 1,200 s, Ψ = 371.5 K.

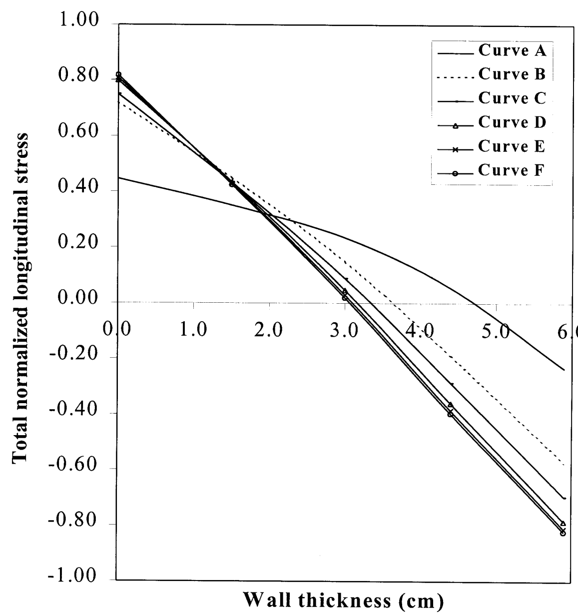

Figure 8b. Wetted wall, normalized total longitudinal stress profiles at different times during blowdown under fire.

Curve A: 38 s, Ψ = 309.1 K; Curve B: 300 s, Ψ = 358.4 K; Curve C: 600 s, Ψ = 383.9 K; Curve D: 900 s, Ψ = 385.0 K; Curve E: 1,100 s, Ψ = 377.3 K; Curve F: 1,200 s, Ψ = 371.5 K.

blowdown of the same vessel under ambient conditions where rupture is most likely in the wetted section at approximately the same time.

Conclusion

This work describes the development of a robust numerical simulation for predicting the risk of rupture following blowdown of pressurized cylindrical vessels containing multicomponent hydrocarbon mixtures under fire attack.

Despite the fact that the most likely and potentially catastrophic blowdown scenario would involve a fire, all such modeling work up to the present time has been confined to blowdown under ambient conditions.

Apart from predicting the precise mode of vessel failure, the simulation is used as an investigative tool for elucidating the role of a number of competing processes that ultimately lead to vessel rupture. In addition, some fundamental differences in the failure risks during blowdown under fire, as opposed to that conducted under ambient conditions, is highlighted. For example, the results of our simulation reveals that thermal radiation, to a large extent, compensates the significant temperature drops which would otherwise occur as a result of the near adiabatic expansion of the fluid inventory during blowdown under ambient surroundings.

In the case of a two-phase gas/liquid inventory, it is found that the much higher heat-transfer coefficient in the liquid phase results in a relatively low inside wall temperature, thus exposing the associated vessel wall to significant thermal stresses. On the other hand, with the vapor being a rather poor medium of heat transfer, it exposes the dry walls to significantly lower temperature gradients, but much higher mean temperatures. The latter results in significant mechanical weakening of the vessel wall.

A detailed analysis of the triaxial thermal and pressure stress profiles reveals that rupture occurs in the dry wall section of the vessel due to the combined effect of the thermally induced mechanical weakening of the vessel walls and the resident total stresses. This is in contrast to the blowdown of the same vessel under ambient conditions where rupture due to low-temperature induced ductile/brittle transition may occur in the wetted wall section.

At no stage do the vessel wall temperatures reach anywhere near the ductile/brittle transition temperature of the vessel material during blowdown under fire, and this suggests that depressurization may be performed as fast as possible. This is, of course, on the premise that the necessary provisions exist for handling or storing the fast flowing inventory. The mathematical model presented in this study serves as a powerful tool for indicating the minimum depressurization rate required in order to eliminate the risk of vessel rupture during blowdown under fire.

Notation

a = vessel inside radius
A = area
b = vessel outside radius
E = modulus of elasticity
G = orifice mass-flow rate
h_a = inside wall heat-transfer coefficient
h_b = inside wall heat-transfer coefficient
J_n = nth order Bessel function of the first kind
k = thermal conductivity
M_D = orifice discharge mass
$N(\beta_m)$ = normalized integral (norm)
P = pressure
Q_f = external heat flux (fire)
r = radius
R_o = eigenfunction
S = entropy
t = time duration
T = temperature
T_h = homogeneous temperature
T_o = temperature at zero time
T_S = steady-state temperature
T_w = wall temperature
Y_n = nth order Bessel function of the second kind
Z = phase
α = thermal diffusivity
β_m = eigenvalue
Ψ = integral wall temperature
τ = coefficient of thermal expansion
ν = poisson's ratio
σ_t^T = tangential thermal stress
σ_r^T = radial thermal stress
σ_l^T = longitudinal thermal stress
σ_t^P = tangential pressure stress
σ_r^P = radial pressure stress
σ_l^P = longitudinal pressure stress

Literature Cited

"API Recommended Practice 520," *Sizing, Selection, and Installation of Pressure Relieving Devices in Refineries,* 5th ed., Amer. Petrol. Inst. (1990a).

"API Recommended Practice 521," *Guide for Pressure-Relieving and Depressuring Systems,* 3rd ed., 19, Amer. Petrol. Inst. (1990b)

Assael, M. J., J. P. Martin Trusler, and T. Tsolakis, *Thermophysical Properties of Fluids*, Imperial College Press, London (1996).

Barlas, S., "Pipeline Safety Law Reauthorization," *Pipeline and Gas J.*, **226**, 6 (Apr. 1999).

Bett, K. E., J. S. Rowlinson, and G. Saville, *Thermodynamics for Chemical Engineers*, Athlone, London (1975).

Beynon, G. V., L. T. Cowley, L. M. Small, and I. Williams, "Fire Engulfment of LPG Tanks: HEATUP, A Predictive Model," *J. of Hazardous Materials*, **20**, 227 (1988).

Birk, A. M., "Scale Effects of Fire Exposure of Pressure-Liquefied Gas Tanks," *J. Loss Prev. Process Ind.*, **8**, 275 (1995).

Birk, A. M., "Modelling the Response of Tankers to External Fire Impingement," *J. Hazard. Mater.*, **20**, 197 (1988).

Brandes, E. A., (ed.), *Smithells Metals Reference Book*, Butterworths, London (1983).

deReuck, K. M., R. J. B. Craven, and A. E. Elhassan, *Transport Properties of Fluids: Their Correlation, Prediction and Estimation*, J. Millat, J. H. Dymond, and C. A. Nieto de Castro, eds., IUPAC, Cambridge Univ. Press, Cambridge (1996).

Haque, M. A., S. M. Richardson, and G. Saville, "Blowdown of Pressure Vessels. I. Computer Model," *Trans IChemE Part B: Process Safety Environmental Protection*, 70 (1992a).

Haque, M. A., S. M. Richardson, G. Saville, G. Chamberlain, and L. Shirvill, "Blowdown of Pressure Vessels. II. Experimental Validation of Computer Model and Case Studies," *Trans. IChemE Part B: Process Safety Environmental Protection*, 70 (1992b).

Hunt, D. L. M., and P. K. Ramskill, "The Behavior of Tanks Engulfed in Fire—The Development of a Computer Program," *IChemE Symp. Ser.*, No. 93, 71 (1985).

Incropera, F. P., and D. P. De Witt, *Fundamentals of Heat and Mass Transfer*, 4th ed., Wiley, New York (1996).

Kielec, D. J., and A. M. Birk, "Analysis of Fire-Induced Ruptures of 400-L Propane Tanks," *J. Pres. Vessel Tech.*, **119**, 365 (1997).

Mahgerefteh, H., P. Saha, and I. G. Economou, "A Study of the Dynamic Response of Emergency Shut-Down Valves Following Full Bore Rupture of Long Pipelines," *Trans. I. Chem.E: Process Safety and Environmental Protection*, **75**, 201 (1997).

Mahgerefteh, H., and S. M. A. Wong, "A Numerical Blowdown Simulation Incorporating Cubic Equations of State," *Comp. and Chem.* Eng., 23 (1999).
Mahgerefteh, H., P. Saha, and I. G. Economou, "Fast Numerical Simulation for Full Bore Rupture of Pressurized Pipelines," *AIChE J.*, **45**, 1191 (1999).
Mahgerefteh, H., P. Saha, and I. G. Economou, "Modelling Fluid Phase Transition Effects on the Dynamic Behavior of ESDV," *AIChE J.*, **46**, 997 (2000).
Michelsen, M. L., "The Isothermal Flash Problem: I. Stability," *Fluid Phase Equil.*, **9**, 1 (1982).
Moodie, K., K. Billinge, and D. P. Cutler, "The Fire Engulfment of LPG Storage Tanks," *IChemE Symp. Ser.*, No. 193, 87 (1985).
Moodie, K., L. T. Cowley, R. B. Denny, L. M. Small, and I. Williams, "Fire Engulfment Tests on a 5 Tonne LPG Tank," *J. Hazardous Mat.*, **20**, 55 (1988).
NAG Fortran Library, Mark 16, *The Numerical Algorithms Group Limited*, Oxford, UK (1993).
Overa, S. J., E. Stange, and P. Salater, "Depressurization of Temperatures and Flare Rates During Depressurisation and Fire," *Proc. GPA Ann. Convention*, 235 (1994).
Ozisik, M. N., *Heat Conduction*, Wiley, New York (1980).
Peng, D. Y., and D. B. Robinson, "A New Two-Constant Equation of State," *Ind. Eng. Chem. Fund.*, **15**, 59 (1976).
Perry, R. H., and D. W. Green, *Perry's Chemical Engineering Handbook*, 7th ed., McGraw-Hill, New York (1997).
Popov, E. P., *Engineering Mechanics of Solids*, Prentice Hall, Englewood Cliffs, NJ (1999).
Ramskill, P. K., "A Description of the 'ENGULF' Computer Codes —Codes to Model the Thermal Response of an LPG Tank Either Fully or Partially Engulfed by Fire," *J. of Hazardous Mat.*, **20**, 177 (1988).
Sumathipala, U. K., G. V. Hadjisophocleous, N. U. Aydemir, C. M. Yu, A. C. M. Sousa, F. R. Steward, and J. E. S. Venart, "Fire Engulfment of Pressure-Liquefied Gas Tanks: Experiments and Modeling," *Fire Hazard and Fire Risk Assessment*, ASTM STP, **1150**, 100 (1992).
Szczepanski, R., "Simulation Programs for Blowdown of Pressure Vessels," IChemE SONG Meeting, London (Apr. 12, 1994).
Timoshenko, S. P., and J. N. Goodier, *Theory of Elasticity*, McGraw-Hill, New York (1987).

Appendix

The eigenfunctions $R_0(\beta_m,r)$, the norm $N(\beta_m)$ and eigenvalues β_m, are given as

$$R_0(\beta_m,r) = S_0 J_0(\beta_m r) - V_0 Y_0(\beta_m r)$$

$$\frac{1}{N(\beta_m)} = \frac{\pi^2}{2}\frac{\beta_m^2 U_0^2}{B_b U_0^2 - B_a V_0^2}$$

$\beta_m s$ (the eigenvalues) are the positive roots of the following transcendental equation

$$S_0 U_0 - V_0 W_0 = 0$$

where

$$U_0 = -J_1(\beta_m a) - \left(\frac{h_a}{\beta_m k}\right) J_0(\beta_m a);$$

$$V_0 = -J_1(\beta_m b) + \left(\frac{h_b}{\beta_m k}\right) J_0(\beta_m b)$$

$$W_0 = -Y_1(\beta_m a) - \left(\frac{h_a}{\beta_m k}\right) J_0(\beta_m a);$$

$$S_0 = -Y_1(\beta_m b) + \left(\frac{h_b}{\beta_m k}\right) Y_0(\beta_m b)$$

$$B_b = 1 + \left(\frac{h_b}{\beta_m k}\right)^2; \quad B_a = 1 + \left(\frac{ha}{\beta_m k}\right)^2$$

For an external heat flux, $h_b = 0$.

J_n is the nth order Bessel function of the first kind, while Y_n is the nth order Bessel function of the second kind.

The tangential, radial, and longitudinal thermal stresses for transient thermal stresses in a hollow cylinder are, respectively, given by (Timoshenko and Goodier, 1987)

$$\sigma_t{}^T = \frac{\tau E}{1-\nu}\frac{1}{r^2}\left[\frac{r^2+a^2}{b^2-a^2}\int_a^b Trdr + \int_a^r Trdr - Tr^2\right]$$

$$\sigma_r{}^T = \frac{\tau E}{1-\nu}\frac{1}{r^2}\left[\frac{r^2-a^2}{b^2-a^2}\int_a^b Trdr - \int_a^r Trdr\right]$$

$$\sigma_l{}^T = \frac{\tau E}{1-\nu}\left[\frac{2}{b^2-a^2}\int_a^b Trdr - T\right]$$

where τ, E, and ν are the coefficient of thermal expansion, modulus of elasticity, and Poisson's ratio, respectively.

The corresponding pressure stresses in a thick-walled cylinder with closed ends are, respectively, given by (Popov, 1999)

$$\sigma_t{}^p = \frac{Pa^2}{b^2-a^2}\left(1+\frac{b^2}{r^2}\right)$$

$$\sigma_r{}^p = \frac{Pa^2}{b^2-a^2}\left(1-\frac{b^2}{r^2}\right)$$

$$\sigma_l{}^p = \frac{Pa^2}{b^2-a^2}$$

Manuscript received Apr. 10, 2001, and revision received Aug. 30, 2001.